Journal of Molecular Spectroscopy 363 (2019) 111182

Contents lists available at ScienceDirect

Journal of Molecular Spectroscopy

journal homepage: www.elsevier.com/locate/jms

Two-color resonance enhanced two-photon ionization and mass analyzed threshold ionization spectroscopy of 2-methoxybenzonitrile

Yan Zhao [a], Yinghui Jin [a], Changyong Li [a,b,*], Suotang Jia [a,b]

[a] State Key Laboratory of Quantum Optics and Quantum Optic Devices, Institute of Laser Spectroscopy, Shanxi University, Taiyuan, Shanxi 030006, China
[b] Collaborative Innovation Center of Extreme Optics, Shanxi University, Taiyuan, Shanxi 030006, China

ARTICLE INFO

Article history:
Received 14 June 2019
In revised form 11 August 2019
Accepted 12 August 2019
Available online 13 August 2019

Keywords:
2-Methoxybenzonitrile
Two-color resonance enhanced two-photon ionization
Mass analyzed threshold ionization
Franck-Condon simulation
Cationic vibronic spectra

ABSTRACT

We report the two-color resonance enhanced two-photon ionization (R2PI) and mass analyzed threshold ionization (MATI) spectra of 2-methoxybenzonitrile. The origin band of $S_1 \leftarrow S_0$ transition and accurate adiabatic ionization energy of 2-methoxybenzonitrile are determined to be 34,176 ± 2, and 70,658 ± 5 cm^{-1}, respectively. The Franck-Condon simulations of the vibrationally resolved electronic spectra for $S_1 \leftarrow S_0$ and $D_0 \leftarrow S_1$ transitions are calculated and used to assist the assignments of the vibronic bands in the experimental spectra. The active vibrations in the S_1 and D_0 states are mainly associated with the motions of the in-plane ring deformation and the in-plane ring-OCH_3 bending. A propensity rule of $\Delta v = 0$, observed in the MATI spectra recorded via different intermediate states, suggests that the molecular geometry of 2-methoxybenzonitrile in the D_0 state resembles that in the S_1 state. Comparing the transition energies of 2-methoxybenzonitrile with those of anisole, benzonitrile and *ortho* substituted derivatives provides insight into the substitution effect of CN and OCH_3 groups on the transition energies.
© 2019 Elsevier Inc. All rights reserved.

1. Introduction

Vibronic spectra of benzonitrile and its derivatives are important for studying their photochemical and photophysical properties, such as the intramolecular charge transfer [1–4], hydrogen-bonding interaction [5–7], and so on. In recent years, the vibrational properties of benzonitrile and its derivatives in the first electronic excited state S_1 and the cationic ground state D_0 have been studied by various spectroscopic technologies [8–13]. The laser induced fluorescence (LIF) excitation, resonance enhanced multiphoton ionization (REMPI), mass analyzed threshold ionization (MATI) and zero kinetic energy (ZEKE) photoelectron spectroscopy have been applied to benzonitrile, benzonitrile-Ar cluster [8,10,14], tolunitrile [11], aminobenzonitrile [12,13,15,16], and fluorobenzonitrile [17,18] to obtain the excitation energies of $S_1 \leftarrow S_0$ transition, the ionization potentials and the vibrational features in the S_1 and D_0 states. In 2015 Arivazhagan group reported the Raman and IR spectra of 2-methoxybenzonitrile for studying the vibrational features in the neutral electronic ground state S_0 [19]. Alvarez-Valtierra and co-workers recently measured the rovibronically resolved fluorescence excitation spectra and dispersed fluorescence emission spectra of 2- and 3-tolunitrile to analyze the internal rotation of methyl group and the geometry in the S_1 state [20,21]. To our best of knowledge, the detailed spectroscopic features of 2-methoxybenzonitrile in the first excited state S_1 and the cationic ground state D_0 are still unavailable in the literature.

In this paper, 2-methoxybenzonitrile molecule in the supersonic jet has been studied using two-color resonance enhanced two-photon ionization (R2PI) and mass analyzed threshold ionization (MATI) spectroscopy. High resolution vibrational spectra for the S_1 and D_0 state are obtained. The observed vibronic bands are assigned by comparing the experimental spectra with the Franck-Condon calculations. With the aid of the quantum chemical calculations, we also analyze the geometrical changes of 2-methoxybenzonitrile induced by the electronic excitation and the ionization processes. The substitution effect of CN and OCH_3 groups on the transition energies is discussed.

2. Experimental and computational details

2.1. Experimental methods

2-methoxybenzonitrile was purchased from Sigma Aldrich (99% purity) and used without further purification. The experimental setup consists of two tunable UV lasers and a time-of-flight (TOF) mass spectrometer as described in previous papers [15,17,22]. Briefly, the vapor of the sample, which was heated to 70 °C, was

* Corresponding author at: State Key Laboratory of Quantum Optics and Quantum Optic Devices, Institute of Laser Spectroscopy, Shanxi University, Taiyuan, Shanxi 030006, China.
E-mail address: lichyong@sxu.edu.cn (C. Li).

https://doi.org/10.1016/j.jms.2019.111182
0022-2852/© 2019 Elsevier Inc. All rights reserved.

seeded in argon gas (2 bar) and then expanded into a high vacuum chamber ($\sim 10^{-4}$ Pa) through a pulsed valve (Parker valve) with a 0.8 mm diameter nozzle and an opening time of 200 μs. The central region of the generated supersonic jet was selected through a 1 mm diameter skimmer located about 20 mm downstream from the nozzle orifice. The pressure in the ionization chamber was maintained at $\sim 10^{-5}$ Pa. Two tunable UV lasers used for excitation and ionization lasers, were produced by the frequency-doubled output of two tunable dye lasers (Sirah: CBR-D-24 and PrecisionScan-D) pumped by the third harmonic of two Nd:YAG lasers (Spectra Physics: INDI-40-10 and Quantel: Q-smart 850), respectively. These two counter-propagating UV lasers were perpendicularly intersected with the molecular beam, and their wavelengths were calibrated with a wavelength meter (HighFinesse WS7-60 UV-I).

The two-color R2PI spectrum was obtained by scanning the excitation laser in the 284–293 nm and fixing the ionization laser to 272 nm. Prior to the MATI experiments, the photoionization efficiency (PIE) measurement was performed to give an approximated value for the ionization energy of 2-methoxybenzonitrile. In the MATI experiments, the excitation laser was used to excite the neutral molecules from the ground state S_0 to a particular vibronic level in the S_1 state. Then, the ionization laser was scanned to excite the molecule in the S_1 state to high-*n* Rydberg states. About 180 ns after the laser pulses, a weak electric field pulse of −1.4 V/cm was applied to remove the direct ions. The molecules in high-*n* Rydberg state with a long lifetime [23] kept moving in the molecular beam and then were ionized by a second electric field pulse of 140 V/cm. The formed MATI ions were accelerated by a voltage of 400 V, then go through a field-free region of about 48 cm long. Finally, they are detected by a dual-stacked microchannel plate detector. The signal from the detector was processed by a multichannel scaler (SRS: SR430) and recorded by a computer. The time sequence of the entire system was controlled by a pulse delay generator (SRS: DG645).

2.2. Computational methods

In order to investigate the vibronic features in the R2PI and MATI spectra of 2-methoxybenzonitrile, the quantum chemical calculations and Franck-Condon simulations have been performed using the Gaussian 09 program package [24]. The geometry optimizations and vibrational frequency calculations of 2-methoxybenzonitrile in the electronic ground state S_0 and the cationic ground state D_0 were carried out using the density functional theory (DFT) with the B3LYP functional and aug-cc-pVDZ basis set. For the first electronic excited state S_1, we performed the time-dependent density functional theory (TD-DFT) calculations with the aug-cc-pVDZ basis set. The calculated vibrational frequencies based on the harmonic approximation were scaled by 0.9736 and 0.9880 for S_1 and D_0 states, respectively, to correct the deviations resulting from the neglect of anharmonic effects, the incomplete treatment of electron correlation and the use of a finite basis set [25]. The vibrationally resolved electronic spectra of 2-methoxybenzonitrile for both transitions of the $S_1 \leftarrow S_0$ and $D_0 \leftarrow S_1$ have also been simulated based on quantum chemistry calculations above and the Franck-Condon approximation (the nuclear positions are nearly unaltered during electronic transition) without considering the Herzberg-Teller coupling [26–28]. The more details on this calculation can be found in Ref. [28].

3. Results

3.1. Two-color R2PI spectrum of 2-methoxybenzonitrile

The structure of 2-methoxybenzonitrile is shown in Fig. 1. Its stable geometry will be discussed in Section 4. The two-color

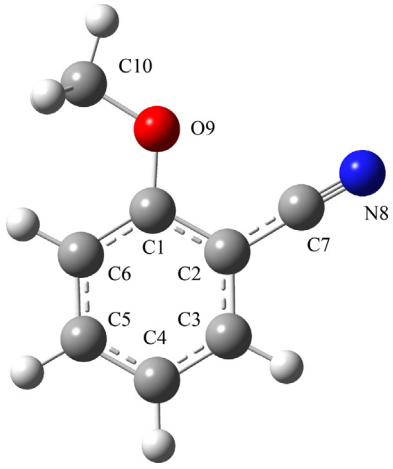

Fig. 1. Molecular structure and numbering of atoms of 2-methoxybenzonitrile in the ground electronic state S_0.

R2PI spectrum of 2-methoxybenzonitrile near the origin of its $S_1 \leftarrow S_0$ electronic transition was recorded by fixing the ionization laser to 272 nm (36765 cm^{-1}) and scanning the excitation laser in the range of 284–293 nm (35211–34130 cm^{-1}). The ionization laser was spatially and temporally overlapped with the excitation laser. The result is shown in Fig. 2a. The most intense band at 34,176 cm^{-1} is assigned to the origin 0_0^0 of the $S_1 \leftarrow S_0$ transition. 2-methoxybenzonitrile belongs to the C_s point group. It has 45 normal vibrational modes, which include 3 cyano, 12 methoxy and 30 benzenelike vibrations. According to the Franck-Condon approximation, only those vibronic transitions with large Franck-Condon factors can be observed in the experiment [26,29]. The simulated spectra can give insight into the vibrational components of the vibronic transitions, and are useful for assigning the observed bands in the experiment [27]. Therefore, the Franck-Condon simulation of the $S_1 \leftarrow S_0$ electronic transition is performed, and the results together with the measured R2PI spectrum are shown in Fig. 2 for comparison. The main peaks at 129, 407, 534, 686, 796, 813 cm^{-1} in the experimental spectrum match well with the calculate bands at 131, 406, 542, 690, 788, and 812 cm^{-1}, respectively.

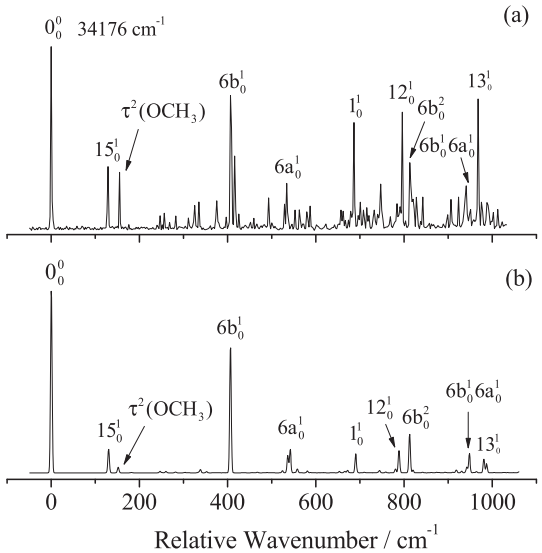

Fig. 2. Two-color REMPI spectrum of 2-methoxybenzonitrile measured by fixing the ionization laser at 272 nm and scanning the excitation laser between 283 and 293 nm (a) and its Franck-Condon simulation (b).

In addition, due to the limitation of the Franck-Condon approximation [27], some weak peaks in the experimental REMPI spectra are not present in the FC simulation. Although the intensities of the simulated bands in the range of 600–1000 cm^{-1} are somewhat underestimated compared with the observed ones, the main spectral profile of the R2PI spectrum is qualitatively reproduced by the Franck-Condon simulation.

On the basis of the simulated spectrum and the previous results on anisole [27,30] and benzonitrile [8,14], the vibrations of 2-methoxybenzonitrile in the S_1 state are assigned. The measured vibrational frequencies in the R2PI spectrum are listed in Table 1 along with the calculated frequencies, possible assignments, and the signal intensities normalized to the origin band.

The Varsanyi/Wilson mode labels [31,32] and the new labeling system [33] are used to label the vibrational modes of 2-methoxybenzonitrile. Most of the observed vibrations in the R2PI spectrum are associated with the totally symmetric vibrational a' modes. The strong bands at 129, 407, 534, 686, 796, and 968 cm^{-1} are assigned to the transitions 15_0^1, $6b_0^1$, $6a_0^1$, 1_0^1, 12_0^1, and 13_0^1, respectively. Modes 6b, 6a, 1, 12, and 13 mainly involve the in-plane ring deformation. Mode 15 is related to the substitute-sensitive in-plane ring-OCH_3 and ring-CN bending motions. The bands located at 247 and 580 cm^{-1} correspond to the in-plane ring-OCH_3 bending β(OCH_3) and ring-CN bending β(CN), respectively. Some weak vibrations with a'' symmetry are also observed in the R2PI spectrum. The low-frequency peak at 155 cm^{-1} is assigned to the OCH_3 group torsion $\tau^2(OCH_3)$. The vibrational modes related to out-of-plane ring deformation appear at 375, 563, 747 cm^{-1}, which are assigned to $16a_0^1$, 4_0^1, and $17b_0^1$ transitions, respectively.

3.2. MATI spectra of 2-methoxybenzonitrile via different intermediate states

Fig. 3 shows the photoionization efficiency curve (PIE) of 2-methoxybenzonitrile via the $S_1 0^0$ intermediate state. The ascending step gives the ionization energy (IE) of 70,660 cm^{-1} with an uncertainty of 10 cm^{-1}. In comparison with PIE, the MATI method gives a sharp peak at the ionization threshold and yields a more definitive value [34]. MATI spectroscopy provides information about the active vibrations of the cation with a higher spectral resolution than the conventional photoelectron spectroscopy. The MATI spectrum of 2-methoxybenzonitrile via the $S_1 0^0$ is shown in Fig. 4a. The most intense peak corresponds to the origin of the transition $D_0 \leftarrow S_1$ of 2-methoxybenzonitrile. Therefore, the adiabatic IE, including the correction for Stark effect [35], is determined to be 70,658 ± 5 cm^{-1} (8.7605 ± 0.0006 eV). The calculated vibrationally resolved electronic spectrum of the transition $D_0 \leftarrow S_1$ is

Table 1
Experimental and calculated vibrational frequencies (in cm^{-1}), intensities and assignments of 2-methoxybenzonitrile in the first electronically excited state S_1.

Cal.[a]	Exp.[a]	Exp. Rel. Int	Assignment and approximate description[b]	D_i[c]
0	0	100	0_0^0, band origin	
131	129	35	15_0^1, β(C—CN), β(C—OCH_3)	D_{21}
152	155	32	$\tau^2(OCH_3)$	
246	247	8	β(OCH_3)	
262	257	10	$16b_0^1$, γ(CCC)	D_{28}
	283	8	$15_0^1\tau^2(OCH_3)$	
	325	14	τ(OCH_3)β(OCH_3)	
338	335	16	$16b_0^1\tau(OCH_3)$	
390	375	17	$16a_0^1$, γ(CCC)	D_{27}
406	407	74	$6b_0^1$, β(CCC)	D_{19}
	416	41	$15_0^1\tau^2(OCH_3)$	
482	493	18	$6b_0^1\tau(OCH_3)$	
536	529	15	$6b_0^1 15^1$	
542	534	26	$6a_0^1$, β(CCC)	D_{18}
	553	12	$6b_0^1\tau^2(OCH_3)$	
558	563	12	4_0^1, γ(CCC)	D_{26}
581	580	11	β(CN)	
	587	14	$16b_0^1\tau(OCH_3)\beta(OCH_3)$	
670	658	12	$6a_0^1 15^1$	
690	686	59	1_0^1, breathing	D_{17}
697	701	16	$6a_0^1\tau^2(OCH_3)$	
	715	13	$\beta(CN)15_0^1$	
	732	12	$\beta(CN)\tau^2(OCH_3)$	
758	747	26	$17b_0^1$, γ(CH)	D_{23}
780	784	15	$16a_0^2$	
788	796	65	12_0^1, β(CCC)	D_{16}
812	813	37	$6b_0^2$	
	827	18	β(CN)β(OCH_3)	
	843	19	$\beta(CN)16b_0^1$	
918	906	17	$12_0^1 15_0^1$	
930	924	19	$6b_0^1 16b_0^2$	
948	941	25	$6b_0^1 6a_0^1$	
981	968	72	13_0^1, β(CCC)	D_{12}
986	975	16	$18b_0^1$, β(CH)	D_{15}
988	988	15	$\beta(CN)6b_0^1$	

[a] The experimental values are shifts from 34176 cm^{-1}, whereas the calculated ones are obtained from the TD-B3LYP/aug-cc-pVDZ calculation, scaled by 0.9736.
[b] ν, stretching; β, in-plane bending; γ, out-of-plane bending; τ, torsion.
[c] The labeling scheme based on Wright's method in Reference [33].

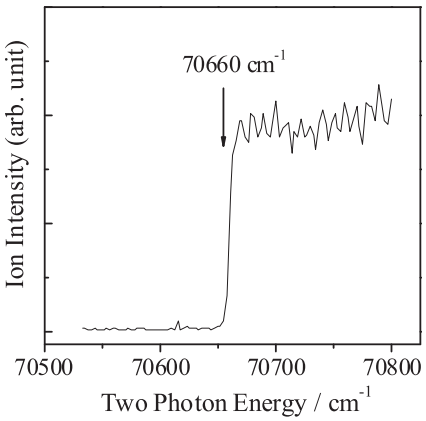

Fig. 3. Photoionization efficiency curve of 2-methoxybenzonitrile recorded via the $S_1 0^0$ intermediate state.

shown in Fig. 4b for comparison with the experimental result. It can be seen that the Franck-Condon simulation reproduces the main spectral features of the experimental spectrum, which is used as a good reference for assigning the observed cationic vibrational bands of 2-methoxybenzonitrile. Similar to the experimental results, the spectral profile of the simulated spectrum is dominated by the vibrationless band 0^+. The MATI peaks at 123, 417, 559, 711, 956, and 1589 cm^{-1} correspond to the simulated bands located at 128 cm^{-1} (15^1), 417 cm^{-1} ($6b^1$), 565 cm^{-1} ($6a^1$), 712 cm^{-1} (1^1), 953 cm^{-1} (13^1), and 1589 cm^{-1} ($8b^1$), respectively, which involve the motions of the in-plane ring deformation. The MATI bands at 236 and 1278 cm^{-1} assigned to the in-plane OCH_3 bending β(OCH_3) and O—CH_3 stretching ν(O—CH_3), are in line with the calculated ones at 237 and 1276 cm^{-1}, respectively. These vibrations are in-plane bending or stretching motion and belong to the totally symmetric a' modes, [36,37]. The experimental and calculated frequencies and assignments of the cationic vibrations are summarized in Table 2.

The MATI spectra of 2-methoxybenzonitrile recorded via the $S_1\tau^2(OCH_3)$, $S_1 6b^1$, and $S_1 1^1$ intermediate states are shown in Fig. 5. The notable features of these cationic spectra are that the most intense bands are assigned to the same vibrational modes as their corresponding intermediate states. This $\Delta\upsilon = 0$ propensity rule maintains a correlation between the excited and cationic vibrations, which has been reported for other benzene derivatives [38–40]. Therefore, in the MATI spectra, a lot of observed bands could be assigned as the combination containing the same mode as the intermediate state [41], as listed in Table 2. When the $6b^1$ and 1^1 modes (which involve the in-plane ring deformation) are used as the intermediate states, the prominent peaks have the a' symmetry.

4. Discussion

4.1. Structure and vibrations of 2-methoxybenzonitrile in S_1 and D_0 states

The *ortho*-substitued anisole derivatives may have different isomers depending on the relative orientation of the methoxy group

Table 2
Experimental and calculated vibrational frequencies (in cm^{-1}) and assignments of 2-methoxybenzonitrile in the cationic ground state D_0.[a]

Intermediate level in the S_1 state				Cal.[a]	Assignment and approximate	D_i[c]
0^0	$\tau^2(OCH_3)$	$6b^1$	1^1		Description[b]	
96				99	τ (OCH_3)	
123				128	15^1, β(C—CN), β(C—OCH_3)	D_{21}
	195			198	$\tau^2(OCH_3)$	
	227				τ (OCH_3) 15^1	
236				237	β(OCH_3)	
	315				$\tau^2(OCH_3)$ 15^1	
338					τ (OCH_3)β(C—OCH_3)	
400		399		401	$9b^1$, β(C—CN), β(C—OCH_3)	D_{20}
417		418		417	$6b^1$, β(CCC)	D_{19}
	436				$\tau^2(OCH_3)$β(OCH_3)	
444				450	$16b^1$τ (OCH_3)	
502					$9b^1$τ (OCH_3)	
		540			$6b^1 15^1$	
559				565	$6a^1$, β(CCC)	D_{18}
568			564	583	β(CN)	
			700		β(CN) 15^1	
711			711	712	1^1, breathing	D_{17}
	755				$\tau^2(OCH_3)$ $6a^1$	
785				790	12^1, β(CCC)	D_{16}
796				803	$6a^1$β(OCH_3)	
		838			$6b^2$	
	904				$\tau^2(OCH_3)$ 1^1	
956				953	13^1, β(CCC)	D_{12}
		974			$6b^1 6a^1$	
1001				1005	$18b^1$, β(CH)	D_{15}
1113				1117	$18a^1$, β(CH)	D_{14}
			1122		$1^1 6b^1$	
		1129			$6b^1 1^1$	
	1150				$\tau^2(OCH_3)$ 13^1	
			1268		$1^1 6a^1$	
1278				1276	ν(O—CH_3)	
		1374			$6b^1 13^1$	
			1422		1^2	
1589				1589	$8b^1$, β(CCC)	D_6

[a] The experimental values are shifts from 70658 cm^{-1}, whereas the predicted ones are obtained from the B3LYP/aug-cc-pVDZ calculations, scaled by 0.9880.
[b] ν, stretching; β, in-plane bending; γ, out-of-plane bending; τ, torsion.
[c] The labeling scheme based on Wright's method in Reference [33].

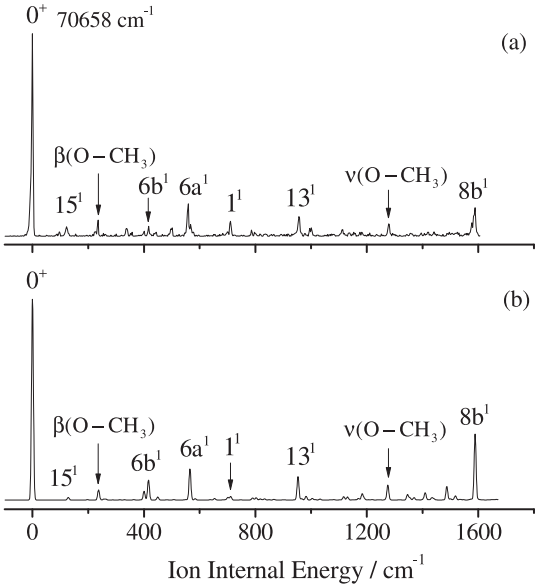

Fig. 4. The MATI spectrum of 2-methoxybenzonitrile recorded via $S_1 0^0$ intermediate state (a) and its Franck-Condon simulation (b).

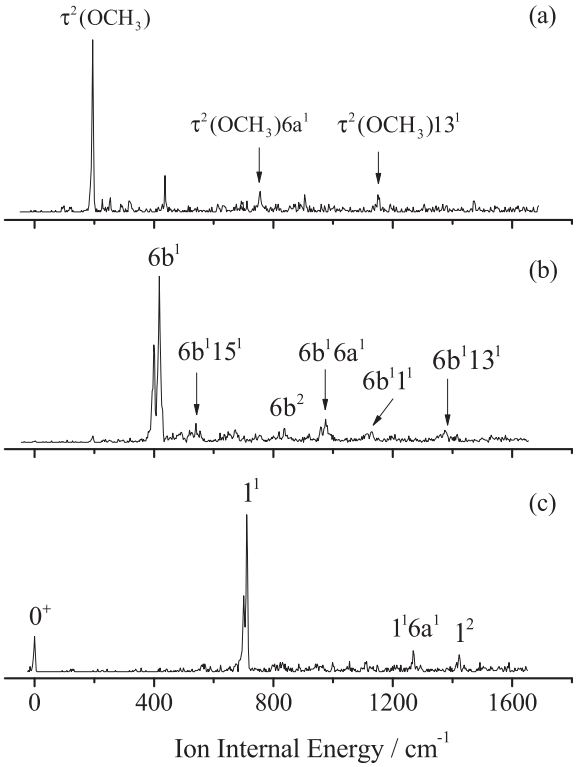

Fig. 5. MATI spectra of 2-methoxybenzonitrile recorded via the $\tau^2(OCH_3)$ (a), $6b^1$ (b), and 1^1 (c) levels in the S_1 state, respectively.

with respect to the substituent. The calculated potential energy curve for the rotation of the methoxy group at the B3LYP/aug-cc-pVDZ level indicates that the planar *trans* form of 2-methoxybenzonitrile is the most stable conformation in the neutral ground state S_0, which is shown in Fig. 1. The other stable conformation is the *non-planar* isomer, where the methoxy group is out of plane of the phenyl ring, and its energy in the S_0 state is higher than that of the *trans* isomer by 1158 cm^{-1}. Therefore, the population of the *non-planar* isomer would be negligibly small in the sample so that it cannot be observed in present experiments. We have also performed geometry optimizations for 2-methoxybenzonitrile in the first electronic excited state S_1 and in the cationic ground state D_0. However, *trans* isomer is the only stable conformation in the S_1 state, and the planar *trans* and *cis* isomers are stable in the D_0 state. The calculated results suggest that only the *trans* conformer of 2-methoxybenzonitrile involves in the $S_1 \leftarrow S_0$ photoexcitation and the $D_0 \leftarrow S_1$ photoionization processes. This case is similar to those of 2-chloroanisole and 2-fluoroanisole, in which only one *trans* isomer was found in the LIF, R2PI, and MATI spectra [42–44].

To investigate the changes in the molecular geometry induced upon transitions, the geometry optimizations of 2-methoxybenzonitrile are performed in S_0, S_1 and D_0 states at the B3LYP/aug-cc-pVDZ level. The equilibrium geometries of 2-methoxybenzonitrile in the S_0, S_1, and D_0 states have a C_s symmetry. The optimized geometrical parameters are given in Table 3, together with the displacements upon excitation and ionization compared with the geometry of 2-methoxybenzonitrile in the S_0 state.

The remarkable changes in the molecular geometries induced on the $^1A'S_1 \leftarrow {}^1A'S_0$ electronic transition are the elongations of all CC bonds on the phenyl ring, while the C_1—O_9 and C_2—C_7 bond lengths decrease by 0.014 and 0.030 Å, respectively. Other geometrical changes are the increases of the bond angles $\angle C_6C_1C_2$, $\angle C_3C_4C_5$ and $\angle C_1C_9C_{10}$, and the decrease of the bond angle $\angle C_1C_2C_3$. In the previous studies for anisole [27,45] and benzonitrile [9], the similar structural changes upon electronic excitation have also been reported. The first electronic excited state S_1 of 2-methoxybenzonitrile, according to TDDFT calculation, arises from the LUMO ← HOMO transition with a $\pi\pi^*$ character. On the transition, the decrease of the electronic density on the methoxy group and the π electron excitation on the aromatic ring induce the corresponding changes in the molecular structures. In principle, it might be also interesting to study the time propagation of electron density upon electronic excitation [46,47]. Such geometrical displacements upon electronic excitation could be further responsible for the prominent vibronic bands in the R2PI spectrum associated with the motions of the in-plane ring deformation as well as the methoxy torsion.

The $D_0 \leftarrow S_1$ transition of 2-methoxybenzonitrile involves the removal of one electron, which may lead to the changes in molecular geometry. The $\Delta\upsilon = 0$ propensity in MATI spectra mentioned in Section 3.2 indicates that the molecular geometry of 2-methoxybenzonitrile does not significantly change upon ionization, which can be further confirmed by comparing the calculated geometries of 2-methoxybenzonitrile in the S_1 and D_0 states. The ionization-induced structural displacements mainly include the decreases of the C_2—C_3, C_5—C_6 and C_1—O_9 bond lengths, implying a small contraction of the aromatic ring in size. It should be noted that some vibrational frequencies related to the in-plane ring deformation in the cationic ground state D_0 are slightly higher than those in the first electronic excited state S_1, although the molecular geometries for both states are similar. For example, the 6b, 6a, and 1 vibrational modes appear at 407, 534, and 686 cm^{-1} in the S_1 state, which are less than the corresponding vibrational frequencies of 417, 559, and 711 cm^{-1} in the D_0 state, respectively. This is similar with previously reported molecules [15,22,43]. Because the vibrational frequency could approximately reflect the rigidity of the chemical bond, the increase of the vibration frequencies maybe impliy that the bond strength of the aromatic ring in the D_0 state is slightly stronger than that in the S_1 state resulting from the removal of one electron.

Table 3
Geometrical parameters of 2-methoxybenzonitrile in its electronic ground, first excited and cationic ground states.

	S_0[a]	S_1[b]	D_0[a]	$\Delta(S_1\text{-}S_0)$	$\Delta(D_0\text{-}S_1)$
Bond length (Å)					
C_1—C_2	1.417	1.458	1.461	0.041	0.003
C_2—C_3	1.404	1.427	1.391	0.023	−0.036
C_3—C_4	1.394	1.416	1.402	0.022	−0.014
C_4—C_5	1.397	1.411	1.428	0.014	0.017
C_5—C_6	1.398	1.422	1.375	0.024	−0.047
C_6—C_1	1.402	1.409	1.427	0.007	0.018
C_2—C_7	1.434	1.404	1.422	−0.030	0.018
C_7—N_8	1.163	1.177	1.165	0.014	−0.012
C_1—O_9	1.354	1.340	1.302	−0.014	−0.038
O_9—C_{10}	1.427	1.433	1.461	0.006	0.028
Bond angle (deg)					
$\angle C_1C_2C_3$	119.9	116.1	119.3	−3.8	3.2
$\angle C_2C_3C_4$	120.6	120.3	119.6	−0.3	−0.7
$\angle C_3C_4C_5$	119.3	122.8	121.1	3.5	−1.7
$\angle C_4C_5C_6$	121.1	118.4	121.0	−2.7	2.6
$\angle C_5C_6C_1$	119.9	119.4	118.9	−0.5	−0.5
$\angle C_6C_1C_2$	119.3	123.0	120.2	3.7	−2.8
$\angle C_1O_9C_{10}$	118.7	121.0	122.6	2.3	1.6

[a] B3LYP/Aug-cc-pVDZ calculation.
[b] TD-B3LYP/Aug-cc-pVDZ calculation.

4.2. Excitation and ionization energies of 2-methoxybenzonitrile

Table 4 lists the excitation energies (E_1s) of the $S_1 \leftarrow S_0$ electronic transition and the ionization energies (IEs) of anisole [27,30,45], benzonitrile [8,10] and their *ortho*-substituted derivatives obtained by REMPI, LIF, MATI, ZEKE spectroscopy [15,42–44,48,49]. Generally, the substituent can interact with the aromatic ring by the conjugation (resonance) effect through the π orbital and by the inductive effect through σ bond [50,51]. Therefore it has a profound effect on the transition energy of benzene derivatives. If the interaction between the substituted group and the aromatic ring in the upper electronic state is stronger than that in the lower electronic state, a red shift would occur for the transition energy of the derivative compared with that of the parent molecule [51,52], and vice versa.

In Table 4, the excitation energies (E_1s) of *ortho*-substituted anisole, 2-chloroanisole, 2-methoxybenozitrile, 2-methoxylphenol and 2-methoxylaniline show the red shifts of 638, 2207, 471, and 2508 cm^{-1} with respect to anisole, respectively. The *ortho*-substituted benzonitrile, 2-methoxybenzonitrile and 2-aminobenzonitrile also show the red shifts of 2342 and 5253 cm^{-1} with respect to benzonitrile in the E_1, respectively. Usually the S_1-S_0 transition of benzene derivatives is subject to $\pi^* \leftarrow \pi$ excitation, leading to an expansion of the ring. The substituent has a greater π-electron overlap with the ring in the electronic excited state than in the ground state, which leads to the stronger interaction between the substituent and the aromatic ring in electronic excited state [48–50,53], and results in a red shift in the E_1. However, the E_1 of 2-fluoroanisole is higher than that of anisole, which is due to the fact that the small F atom has a weaker conjugation effect with the aromatic ring than the Cl, CN, OH and NH_2 substituted groups [53–55]. Similar observations have also been found in the 2-fluoroaniline, 2-fluorophenol, 3-fluorophenol, and 3-fluoroanisole molecules [48,56].

As shown in Table 4, the E_2 of 2-methoxylphenol and 2-methoxylaniline are lower than that of anisole by 1933 and 5213 cm^{-1}, respectively. Meanwhile, 2-methoxybenzonitrile and 2-aminobenzonitrile have much smaller E_2 compared with that of benzonitrile (ΔE_2 = −5490, −6584 cm^{-1}). The OH, OCH_3, and NH_2 groups are commonly referred to as the electron-donating groups. The $D_0 \leftarrow S_1$ transition likely involves the removal of one electron of the oxygen or nitrogen atom of the OH, OCH_3, and

Table 4
Measured transition energies (cm^{-1}) of anisole, benzonitrile and their *ortho*-substitued derivatives.[a]

Molecule	$E_1(S_1 \leftarrow S_0)$	ΔE_1	$E_2(D_0 \leftarrow S_1)$	ΔE_2	IE	ΔIE
anisole[b]	36,383	0	30,016	0	66,399	0
2-fluoroanisole[c]	36,609	226	30,745	729	67,354	955
2-chloroanisole[d]	35,745	−638	31,237	1221	66,982	583
2-methoxybenzonitrile[e]	34,176	−2207	36,482	6466	70,658	4259
2-methoxylphenol[f]	35,912	−471	28,083	−1933	63,995	−2404
2-methoxylaniline[g]	33,875	−2508	24,803	−5213	58,678	−7721
benzonitrile[h]	36,518	0	41,972	0	78,490	0
2-methoxybenzonitrile[e]	34,176	−2342	36,482	−5490	70,658	−7832
2-aminobenzonitrile[i]	31,265	−5253	35,388	−6584	66,653	−11837

[a] ΔE_1, ΔE_2, and ΔIE are shifts of E_1, E_2 and IE with respect to anisole or benzonitrile.
[b] Reference [27,30,45].
[c] Reference [42,44].
[d] Reference [43].
[e] This work.
[f] Reference [48].
[g] Reference [49].
[h] Reference [8,10].
[i] Reference [15].

NH_2 groups. The observed red shifts in the energy associated with the $D_0 \leftarrow S_1$ transition (E_2) indicate that the OH, OCH_3, and NH_2 substituted groups cause an increase of the electron density nearby the oxygen or nitrogen atom [49]. In contrast, the CN, F and Cl substituents with the electron-withdrawing nature can decrease the electron density nearby the oxygen of 2-methoxybenzonitrile, 2-fluoroanisole and 2-chloroanisole, and therefore the E_2 of 2-methoxybenzonitrile, 2-fluoroanisole and 2-chloroanisole are greater than that of anisole. The similar cases are also observed in 2-fluorophenol [48] and 2-chloroanisole [43]. The ionization energy IE is given by the sum of the E_1 and E_2. The IE of 2-methoxybenzonitrile is larger than that of anisole, and lower than that of benzonitrile, which indicate that the shift on ionization energy is related to the nature of substituents.

5. Conclusion

The R2PI and MATI spectra of 2-methoxybenzonitrile are measured under the supersonic molecular beam condition. The vibrational features in the S_1 and D_0 states and the geometrical changes upon excitation and ionization are investigated. The band origin of the $S_1 \leftarrow S_0$ electronic transition and adiabatic ionization energy of 2-methoxybenzonitrile are determined to be 34,176 ± 2 and 70,658 ± 5 cm^{-1}, respectively. The Franck-Condon simulations of $S_1 \leftarrow S_0$ and $D_0 \leftarrow S_1$ transitions reproduce qualitatively the main profiles of the experimental spectra, and therefore are used as an aid to assign the observed vibronic bands. Most of active vibrations of 2-methoxybenzonitrile in the S_1 and D_0 states correspond to the motions of the in-plane ring deformation and the in-plane ring-OCH_3 bending. The MATI spectra recorded via different intermediate states show a propensity rule of $\Delta\upsilon = 0$. Thus, there is no remarkable change in the molecular geometries upon ionization. However, some normal vibrational frequencies related to the in-plane ring deformation in the cationic ground state D_0 are higher than those in the first electronic excited state S_1, implying the stronger π bond in the D_0 state. The excitation energy E_1 of 2-methoxybenzonitrile are lower than those of anisole and benzonitrile, which is caused by the dominant conjugation effect. As for the substitution effect on the ionization energy, the electron-withdrawing group CN increases the ionization energy, whereas the electron-donating group OCH_3 reduces the ionization energy.

Acknowledgments

This work was supported by National Key R&D Program of China (Grant No. 2017YFA0304203), National Natural Science Foundation of China (Grants Nos. 61575115, 61835007, 11434007, 61378039), PCSIRT (No. IRT_17R70), 111 project(Grant No. D18001), and the Fund for Shanxi"1331 Project" Key Subjects Construction.

References

[1] J.-K. Lee, T. Fujiwara, W.G. Kofron, M.Z. Zgierski, E.C. Lim, J. Chem. Phys. 128 (2008) 164512.
[2] R.C. Ramos, T. Fujiwara, M.Z. Zgierski, E.C. Lim, J. Phys. Chem. A 109 (2005) 7121–7126.
[3] K.A. Zachariasse, S.I. Druzhinin, S.A. Kovalenko, T. Senyushkina, J. Chem. Phys. 131 (2009) 224313.
[4] A. Perveaux, P.J. Castro, D. Lauvergnat, M. Reguero, B. Lasorne, J. Phys. Chem. Lett. 6 (2015) 1316–1320.
[5] K. Sakota, N. Yamamoto, K. Ohashi, M. Saeki, S.-I. Ishiuchi, M. Sakai, M. Fujii, H. Sekiya, Chem. Phys. 283 (2002) 209–219.
[6] E.S. Kryachko, M.T. Nguyen, J. Chem. Phys. 115 (2001) 833–841.
[7] D.J. Aschaffenburg, R.S. Moog, J. Phys. Chem. B 113 (2009) 12736–12743.
[8] M. Araki, S. Sato, K. Kimura, J. Phys. Chem. 100 (1996) 10542–10546.
[9] R.M. Helm, H.P. Vogel, H.J. Neusser, Chem. Phys. Lett. 270 (1997) 285–292.
[10] C.H. Kwon, H.L. Kim, M.S. Kim, J. Phys. Chem. A 107 (2003) 10969–10975.
[11] K. Suzuki, S. Ishiuchi, M. Sakai, M. Fujii, J. Electron Spectrosc. Relat. Phenom. 142 (2005) 215–221.
[12] L.C.L. Huang, J.L. Lin, W.B. Tzeng, Chem. Phys. 261 (2000) 449–455.
[13] E.M. Gibson, A.C. Jones, D. Phillips, Chem. Phys. Lett. 146 (1988) 270–274.
[14] T. Kobayashi, K. Honma, O. Kajimoto, S. Tsuchiya, J. Chem. Phys. 86 (1987) 1111–1117.
[15] Y. Jin, Y. Zhao, Y. Yang, L. Wang, C. Li, S. Jia, Chem. Phys. Lett. 692 (2018) 395–401.
[16] P. Kolek, K. Pirowska, J. Najbar, Phys. Chem. Chem. Phys. 3 (2001) 4874–4888.
[17] Y. Zhao, Y. Jin, J. Hao, Y. Yang, C. Li, S. Jia, Chem. Phys. Lett. 711 (2018) 127–131.
[18] S. Jiang, D.H. Levy, J. Phys. Chem. A 106 (2002) 8590–8598.
[19] M. Elanthiraiyan, B. Jayasudha, M. Arivazhagan, Spectrochim. Acta A Mol. Biomol. Spectrosc. 134 (2015) 543–552.
[20] J.A. Ruiz-Santoyo, J. Wilke, M. Wilke, J.T. Yi, D.W. Pratt, M. Schmitt, L. Álvarez-Valtierra, J. Chem. Phys. 144 (2016) 044303.
[21] F. Gmerek, B. Stuhlmann, L. Álvarez-Valtierra, D.W. Pratt, M. Schmitt, J. Chem. Phys. 144 (2016) 084304.
[22] Y. Zhao, Y. Jin, J. Hao, Y. Yang, L. Wang, C. Li, S. Jia, Spectrochim. Acta A Mol. Biomol. Spectrosc. 207 (2019) 328–336.
[23] F. Merkt, R.N. Zare, J. Chem. Phys. 101 (1994) 3495–3505.
[24] M.J. Frisch, G.W. Trucks, H.B. Schlegel, G.E. Scuseria, M.A. Robb, et al., Gaussian 09, Revision C.01, Gaussian, Inc, Wallingford, CT, 2009.
[25] P. Sinha, S.E. Boesch, C. Gu, R.A. Wheeler, A.K. Wilson, J. Phys. Chem. A 108 (2004) 9213–9217.
[26] S. Schumm, M. Gerhards, K. Kleinermanns, J. Phys. Chem. A 104 (2000) 10648–10655.
[27] J. Bloino, M. Biczysko, O. Crescenzi, V. Barone, J. Chem. Phys. 128 (2008) 244105.
[28] J.B.V. Barone, M. Biczysko, Vibrationally-resolved electronic spectra in GAUSSIAN 09, GAUSSIAN 09, Revision A.02, 2009, available online at http://dreamsnet.sns.it/sites/default/files/download/docs/vibronic_spectra_G09-A02.pdf.
[29] Y.R. Lee, D.W. Kang, H.L. Kim, C.H. Kwon, J. Chem. Phys. 141 (2014) 174303.
[30] M. Pradhan, C. Li, J.L. Lin, W.B. Tzeng, Chem. Phys. Lett. 407 (2005) 100–104.
[31] G. Varsanyi, Assignments of Vibrational Spectra of Seven Hundred Benzene Derivatives, Wiley, New York, 1974.
[32] E.B. Wilson, Phys. Rev. 45 (1934) 706–714.
[33] W.D. Tuttle, A.M. Gardner, A. Andrejeva, D.J. Kemp, J.C.A. Wakefield, T.G. Wright, J. Mol. Spectrosc. 344 (2018) 46–60.
[34] L. Zhu, P. Johnson, J. Chem. Phys. 94 (1991) 5769–5771.
[35] B. Zhang, C. Li, H. Su, J.L. Lin, W.B. Tzeng, Chem. Phys. Lett. 390 (2004) 65–70.
[36] C.H. Kwon, H.L. Kim, M.S. Kim, J. Chem. Phys. 116 (2002) 10361–10371.
[37] C.H. Kwon, H.L. Kim, M.S. Kim, J. Chem. Phys. 118 (2003) 6327–6335.
[38] S. Kruger, J. Grotemeyer, Phys. Chem. Chem. Phys. 18 (2016) 7100–7113.
[39] S. Krueger, F. Witte, J. Helfrich, J. Grotemeyer, RSC Adv. 5 (2015) 937–948.
[40] C. Harthcock, J. Zhang, W. Kong, Chem. Phys. Lett. 556 (2013) 23–28.
[41] J. Zhang, C. Harthcock, F. Han, W. Kong, J. Chem. Phys. 135 (2011) 244306.
[42] T. Isozaki, K. Sakeda, T. Suzuki, T. Ichimura, J. Chem. Phys. 132 (2010) 214308.
[43] H.C. Huang, B.Y. Jin, W.B. Tzeng, J. Photochem. Photobiol. A Chem. 243 (2012) 73–79.
[44] K.S. Shiung, D. Yu, S.Y. Tzeng, W.B. Tzeng, Chem. Phys. Lett. 524 (2012) 38–41.
[45] C.G. Eisenhardt, G. Pietraperzia, M. Becucci, Phys. Chem. Chem. Phys. 3 (2001) 1407–1410.
[46] J. Manz, J.F. Pérez-Torres, Y. Yang, J. Phys. Chem. A 118 (2014) 8411–8425.
[47] D. Jia, J. Manz, Y. Yang, J. Chem. Phys. 148 (2018) 041101.
[48] L. Yuan, C. Li, J.L. Lin, S.C. Yang, W.B. Tzeng, Chem. Phys. 323 (2006) 429–438.
[49] J.L. Lin, C.J. Huang, C.H. Lin, W.B. Tzeng, J. Mol. Spectrosc. 244 (2007) 1–8.
[50] C. Dong, L. Zhang, S. Liu, L. Hu, M. Cheng, Y. Du, Q. Zhu, C. Zhang, J. Mol. Spectrosc. 292 (2013) 35–46.
[51] P.Y. Wu, S.Y. Tzeng, Y.C. Hsu, W.B. Tzeng, J. Mol. Spectrosc. 332 (2017) 3–7.
[52] W.C. Peng, P.Y. Wu, S.Y. Tzeng, W.B. Tzeng, Chem. Phys. Lett. 700 (2018) 145–148.
[53] J. Huang, J.L. Lin, W.B. Tzeng, Chem. Phys. Lett. 422 (2006) 271–275.
[54] H.C. Huang, K.S. Shiung, B.Y. Jin, W.B. Tzeng, Chem. Phys. 425 (2013) 114–120.
[55] P.Y. Wu, H.H. Huang, K.C. Lin, W.B. Tzeng, Chem. Phys. Lett. 682 (2017) 34–37.
[56] K.S. Shiung, D. Yu, H.C. Huang, W.B. Tzeng, J. Mol. Spectrosc. 274 (2012) 43–47.